

Research Article

## Targeting BUB3 in combination with paclitaxel inhibits proliferation of glioblastoma cells by enhancing cellular senescence

Patrícia M. A. Silva <sup>1,2</sup> , Ana V. Nascimento <sup>1</sup> , Olga Martinho <sup>3,4</sup> , Rui M. Reis <sup>3,4</sup>  and Hassan Bousbaa <sup>1,5\*</sup> 

<sup>1</sup> UNIPRO - Oral Pathology and Rehabilitation Research Unit, University Institute of Health Sciences (IUCS), CESPU, Rua Central de Gandra, 1317, 4585-116 Gandra, Portugal; patricia.silva@cespu.pt; anavanesa65@gmail.com

<sup>2</sup> TOXRUN - Toxicology Research Unit, University Institute of Health Sciences (IUCS), CESPU, Rua Central de Gandra, 1317, 4585-116 Gandra, Portugal.

<sup>3</sup> Life and Health Sciences Research Institute (ICVS), Medical School, University of Minho, Campus de Gualtar, 4710-057 Braga, Portugal; olgamartinho@med.uminho.pt

<sup>4</sup> Molecular Oncology Research Center, Barretos Cancer Hospital, São Paulo 14784-400, Brazil; ruireis.hcb@gmail.com

<sup>5</sup> Interdisciplinary Center of Marine and Environmental Research (CIIMAR), University of Porto, Terminal de Cruzeiros do Porto de Leixões, Av. General Norton de Matos s/n 4450-208 Matosinhos, Portugal.

\* Correspondence: hassan.bousbaa@iucs.cespu.pt

**Abstract:** Glioblastoma (GBM) is the most common malignant primary brain tumor, with remarkably poor prognosis and survival rates. Existing treatments cannot cure GBM patients, and GBM recurrence remains a clinical bottleneck. To explore new GBM chemotherapeutic targets and new therapeutic strategies, the role of the spindle assembly checkpoint (SAC) protein BUB3 in GBM was investigated. We found *BUB3* overexpression to be a common feature in GBM tissues. Moreover, *BUB3* knockdown significantly inhibited proliferation of glioblastoma cells, and enhanced the antiproliferative activity of paclitaxel on these cells, through potentiation of multipolar spindles and SAC weakening. Interestingly, we showed that BUB3 downregulation exerts its antiproliferative activity mainly through induction of premature cellular senescence and, to a lesser extent, through apoptosis. Senescence phenotype, but not apoptosis, was highly potentiated in BUB3-depleted glioblastoma cells treated with clinically relevant doses of paclitaxel. Based on these observations, BUB3 inhibition combined with paclitaxel is suggested as a potentially effective strategy for the treatment of GBM. We propose BUB3 as a novel target and biomarker for GBM.

**Keywords:** glioblastoma; BUB3; paclitaxel; spindle assembly checkpoint; mitosis; senescence

Received: 02 February 2022; Accepted: 02 March 2022; Published: 25 March 2022

### Introduction

Glioblastoma (GBM) is the most aggressive and lethal tumor type from the central nervous system (CNS), and exhibits an impressive aneuploidy with notable tumor heterogeneity [1,2]. The standard treatment of GBM comprises surgery, radiotherapy and concomitant and adjuvant chemotherapy, but no effective treatment exists to date [3,4]. GBM displays a high rate of relapsing, with the patients' median survival being still less than 14 months [5]. Thus, there is a strong interest in understanding the molecular mechanism underlying GBM pathogenesis, with a concomitant strategy towards the development of new therapeutic drugs and biomarkers.

The spindle assembly checkpoint (SAC) is the surveillance mechanism during mitosis that prevents anaphase onset until all chromosomes are properly attached and aligned at the metaphase plate, thus preventing chromosome missegregation and aneuploidy, a hallmark of cancer cells [6]. Indeed, aneuploidy has been increasingly related with SAC defects [6,7].

Budding uninhibited by benomyl 3 (BUB3) was identified in 1991 in the budding yeast *Saccharomyces cerevisiae*, in a genetic screen of genes that play a role in ensuring accurate chromosome segregation [8,9]. BUB3 is required for the recruitment of the SAC proteins budding uninhibited by benzimidazole 1 (BUB1) and budding uninhibited by benzimidazole-related 1 (BUBR1) to unattached kinetochores, the proteinaceous structures built on both sides of the centromere region of the mitotic chromosome, serving as the site of attachment to spindle microtubules. Unattached kinetochores act as platforms of the assembly of the mitotic checkpoint complex (MCC), which inhibits the multi-subunit E3 ubiquitin ligase anaphase-promoting complex/cyclosome (APC/C), thereby inhibiting anaphase onset [7].

Inhibiting BUB3 leads to premature exit from mitosis, resulting in severe chromosome missegregation, and eventually cell death [10]. *BUB3* mutations are not reported in GBM, yet gene upregulation has been found in a variety of human cancers and was associated with poor prognoses, making BUB3 a potential new anticancer target. Currently, there are no BUB3 inhibitors, but BUB3 targeting can be achieved by RNA interference (RNAi) to assess its anti-cancer effects [11–13]. Here, we investigated the role of BUB3 as a new GBM chemotherapeutic target. As paclitaxel effect is synergized by cell division errors, we also explored the potential of BUB3 inhibition to enhance the sensitivity of GBM cells to clinical doses of paclitaxel [14,15].

## Materials and Methods

### Cell culture

U251 and U373 glioblastoma cell lines (kindly provided by Rui M. Reis, ICVS, University of Minho) were grown in Dulbecco's Modified Eagle Medium (DMEM, Merck KGaA, Darmstadt, Germany), supplemented with 10% fetal bovine serum (FBS, Merck). Human astrocytes (Innoprot, Bizkaia, Spain) were grown in astrocyte medium (AM, ScienCell Research Laboratories, San Diego, California) enriched with 2% FBS and 1% of astrocyte growth supplement (AGS, ScienCell Research Laboratories). All cell lines were maintained at 37 °C under a humidified 5% CO<sub>2</sub> atmosphere.

### Quantitative real-time reverse transcriptase polymerase chain reaction (qRT-PCR)

Total cell RNA was obtained with the PureZOL™ RNA Isolation Reagent (Bio-Rad Laboratories, Inc., Hercules, CA, USA), according to the manufacturer's instructions. cDNA synthesis was performed with the iScript™ cDNA Synthesis Kit (Bio-Rad), using total cell RNA as template, following supplier's instructions. For qRT-PCR, cDNA was amplified using the iQ™ SYBR Green Supermix Kit (Bio-Rad) on an iQ Thermal Cycler (Bio-Rad), according to the following program: initial denaturing step at 95.0 °C for 3 min; 40 cycles at 94.0 °C for 20 s; 60.0 °C for 30 s and 72.0 °C for 30 s. The melt curve included temperatures from 65.0 to 95.0 °C, with increments of 0.5 °C for 5 s. Primers for BUB3 were as follows: forward: 5'-GTGTTGGTGTGGGACTTACG-3' and reverse: 5'-GCTTAATACATAACCCTGCTTG-3'; for GAPDH, primers were as follows: forward: 5'-ACAGTCCAGCCGCATCTTC-3' and reverse: 5'-GCCCAATACGACCAAATCC-3'. Data were acquired with the CFX Manager™ Software (version 1.0, Bio-Rad) and the results were analyzed according to the  $\Delta\Delta\text{CT}$  method and normalized against glyceraldehyde 3-phosphate dehydrogenase (GAPDH) expression levels, used as a control template. A fold value of mRNA level  $\geq$  or  $\leq$  1.5 relative to that of normal astrocyte cells was considered as over- or underexpression, respectively.

### UALCAN analysis

We searched the public cancer database, UALCAN, to identify studies with *BUB3* gene expression datasets, and compared the expression of glioblastoma vs. normal brain tissue. To be included, a dataset was required to have significant gene expression with a *p* value < 0.05.

### RNA interference

A total of  $0.1 \times 10^6$  cells was seeded in 22 mm poly-L-lysine-coated coverslips in 6-well plates, allowed to attach for 24 hours, and transfected using INTERFERin siRNA Transfection Reagent (PolyPlus, New York, USA), according to the manufacturer's instructions. Validated small interfering RNA (siRNA) duplexes against *BUB3* (Santa Cruz Biotechnology, Dallas, USA) and a validated negative control siRNA (AllStars Negative Control siRNA, Qiagen, Germantown MD, USA) were used at a final concentration of 6.7 nM.

### Western blotting

Seventy-two hours after siRNA transfection, cells were detached and collected by centrifugation, and resuspended in lysis buffer (50 mM Tris, pH 7.5; 150 mM NaCl; 1 mM EDTA; 1% Triton X-100) containing 1:100 protease inhibitors (104 mM AEBSF, 0.085 mM Aprotinin, 4 mM Bestatin, 1.4 mM E-64, 2 mM Leupeptin, 1.5 mM Pepstatin A; Sigma-Aldrich cocktail P8340). Cell extracts (20 µg) were loaded onto a 4-7.5% acrylamide gradient gel and, then, transferred to a nitrocellulose membrane using the Trans-Blot Turbo Transfer System (Bio-Rad). The membrane was blocked in TBST (50 mM Tris, pH 8.0; 150 mM NaCl; 0.05% Tween-20) plus 5% w/v nonfat dry milk solution, and incubated with the primary antibodies diluted in TBST plus 1% nonfat dried milk. The primary antibodies used were: mouse anti-BUB3 (1:1000, 611731 clone 31, BD Biosciences), mouse anti-CASPASE 3 (1:2000, clone 4-1-18, Merck Millipore) and rabbit anti- $\alpha$ -TUBULIN (1:1500, ab15246, Abcam). Horseradish peroxidase (HRP)-conjugated secondary antibodies were diluted at 1:1500 (anti-mouse, Vector) or at 1:1000 (anti-rabbit, Sigma-Aldrich). The signal was detected using enhanced chemiluminescence (ECL) detection of the HRP-conjugated secondary antibodies. Blots were visualized using X-ray films and the images were captured using Carestream BIOMAX Light Film (Sigma-Aldrich). BUB3 repression was calculated by averaging three independent experiments, using the ImageJ 1.4v software (<http://rsb.info.nih.gov/ij/>) for the quantification of the intensity of the protein signal.  $\alpha$ -Tubulin expression levels were used for normalization.

### Immunofluorescence

Cells were fixed for 12 minutes in freshly prepared 2% paraformaldehyde (Sigma-Aldrich) in phosphate-buffered saline (PBS), rinsed three times in PBS and permeabilized for 7 minutes with 0.5% Triton X-100 in PBS. After PBS washing, cells were blocked for 30 minutes in 10% FBS in PBST (PBS plus 0.05% Tween-20), followed by a 1 hour-incubation with primary antibodies diluted in PBST with 5% FBS. The primary antibodies used were: mouse anti-BUBR1 (1:1000, 612503, BD Biosciences) and human anti-CREST (1:3000, gift from E. Bronze-da-Rocha, IBMC, Porto, Portugal). After PBST washing, cells were incubated with fluorescently-labeled secondary antibodies for 1 hour. All secondary antibodies were diluted at 1:1500 (Molecular Probes). DNA was stained with 2 µg/ml 4',6-diamidino-2-phenylindole (DAPI, Sigma-Aldrich) diluted in Vectashield mounting medium (Vector, H-1000).

### Cell viability assay

Cell viability was determined by the 3-(4,5-dimethylthiazolyl-2)-2,5-diphenyltetrazolium bromide (MTT) assay (Sigma-Aldrich). A total of  $0.05 \times 10^6$  siRNA-transfected cells was seeded in a 96-well plate and 24 hours later treated with 2, 4 and 10 nM of paclitaxel. After 48 hours, 20 µl of the MTT reagent (5 mg/ml in PBS) were added and the cells placed into the cell incubator for 4 hours. The purple formazan precipitate was solubilized with a detergent solution (98% 2-propanol, 10% Triton X-100, 0.037% HCl), and after 2 hours, the optical density was measured at 570 nm in a microplate reader (Biotek Synergy 2) and the % of cell viability determined for each experimental condition.

### TUNEL assay

Seventy-two hours after siRNA transfection, the terminal deoxynucleotidyl transferase-mediated nick end labeling (TUNEL) assay was performed using the DeadEnd Fluorometric TUNEL System (Promega, Madison, WI, USA), according to the manufacturer's instructions. DNA was stained with 2 µg/ml DAPI in Vectashield mounting medium. The % of apoptotic cells was determined by scoring TUNEL-positive cells in a total of 500 cells under fluorescence microscopy, from at least ten random microscopic fields, for each experimental condition.

### Caspase activity measurement

Cells were treated with control- and BUB3-siRNAs for 72 hours, with or without 10 nM of paclitaxel for 48 hours. Following PBS wash, cells were incubated in Glo Lysis Buffer (Promega) for 5 minutes at room temperature, to promote cell lysis. The lysates were collected and frozen at -20 °C. For caspase 3 activity, we used the Ac-DEVD-pNA peptide substrate (Sigma-Aldrich), according to the manufacturer's instructions. Hydrogen peroxide (H<sub>2</sub>O<sub>2</sub>, Sigma-Aldrich) was used at 500 µM as a positive control for apoptosis, and diluted in culture medium immediately before use. The results were normalized against protein content and expressed comparatively to control siRNA-treated cells.

### Clonogenic assay

A total of 500 siRNA-transfected cells was seeded in six-well plates, allowed to attach for 24 hours, and treated with 2 and 4 nM of paclitaxel. Forty-eight hours later, medium with paclitaxel was removed, the cells were washed twice with PBS, then incubated in fresh DMEM, and left for 10 days for colonies to form. The recovered colonies were fixed with 3.7% paraformaldehyde in PBS, for 5 minutes, and stained with 0.05% (w/v) crystal violet (Merck Millipore, Billerica, MA, USA) in distilled water, for 20 minutes. The number of colonies was counted on duplicate dishes, from three independent experiments. The plating efficiency (PE) was calculated as the percentage of the number of colonies formed over the number

of cells seeded, in control siRNA-treated cells. The survival fraction was determined as the number of colonies over the number of cells seeded  $\times$  1/PE, for each condition.

### Microscopy analysis and live-cell image processing

For live-cell imaging experiments, U251 cells were seeded onto LabTek II chambered cover glass (Nunc, Penfield, NY, USA) containing 1 ml of culture medium, and allowed to attach for 24 hours at 37 °C with 5% CO<sub>2</sub>. Later, cells were transfected with control (control siRNA) or BUB3 (siBUB3) siRNAs, or treated with 10 nM of paclitaxel, in complete culture medium. For siBUB3 and paclitaxel co-treatment, paclitaxel 10 nM was added 24 hours after siRNA-transfection. Images were captured at 10 min-intervals up to 72 h under differential interference contrast (DIC) optics, with a 63 $\times$  objective on an Axio Observer Z.1 SD inverted microscope, equipped with an incubation chamber with the temperature set to 37 °C and an atmosphere of 5% CO<sub>2</sub>. Movies were generated from the time-lapse images using the ImageJ software (version 1.44, Rasband, W.S., ImageJ, U. S. National Institutes of Health, Bethesda, MD, USA). The number of cells that were arrested at mitosis, apoptotic, or bypassed cytokinesis was scored.

### Senescence-associated beta-galactosidase (SA- $\beta$ -gal) activity assay

Cells were treated with control- and BUB3-siRNAs for 72 hours, with or without 10 nM of paclitaxel for 48 hours. Then, cells were fixed for 3-5 min (room temperature) in 2% formaldehyde/0.2% glutaraldehyde solution, washed twice in PBS, and incubated at 37 °C with fresh SA- $\beta$ -gal stain solution (50 mg/ml of 5-bromo-4-chloro-3-indolyl P3-D-galactoside (X-Gal); 40 mM citric acid/sodium phosphate, pH 6.0; 5 mM potassium ferrocyanide; 5 mM potassium ferricyanide; 150 mM NaCl; 2 mM MgCl<sub>2</sub>). After 4 hours, cells were observed under phase contrast microscopy and the % of senescent cells (stained blue), over a total of cells, from random microscope fields, was determined.

### Microscopy analysis and image processing

Phase-contrast microscopy images were recorded with a 10 $\times$  objective, on a Nikon TE 2000-U microscope, using a DXM1200F digital camera and with Nikon ACT-1 software (Melville, NY). Fluorescence images were acquired with Plan Apochromatic 63 $\times$ /NA 1.4 objective on an Axio Observer Z.1 SD microscope (Carl Zeiss, Germany), coupled to an AxioCam MR3. Z-stacks were acquired with 0.4  $\mu$ m-intervals and images were processed using ImageJ version 1.44 (<http://rsb.info.nih.gov/ij/>).

### Statistical analysis

Statistical analysis was performed using Unpaired Student t-test, one-way ANOVA with Kruskal–Wallis and Dunn’s multiple correction test or ordinary two-way ANOVA with Tukey’s multiple comparisons test, in GraphPad Prism version 6 (GraphPad software Inc., CA, USA). Data are presented as the means  $\pm$  standard deviation (SD) of at least three independent experiments. The level of significance was set at probabilities of \* $p$  < 0.05, \*\* $p$  < 0.01, \*\*\* $p$  < 0.001 and \*\*\*\* $p$  < 0.0001.

## Results

### BUB3 is upregulated in glioblastoma cells

BUB3 expression levels were determined in the two glioblastoma cell lines, U251 and U373, and compared to normal astrocytes. BUB3 transcript levels in the two cell lines were determined by qRT-PCR. We found a  $4.5 \pm 0.48$  and  $4.6 \pm 0.33$ -fold increase in U251 and U373, respectively, compared to astrocytes (Fig. 1A). BUB3 protein levels were also increased by  $1.58 \pm 0.09$ -fold in U251 cells and by  $1.69 \pm 0.10$ -fold in U373 cells, as revealed by Western blotting analysis (Fig. 1B). We noted that the increase in the expression levels was more pronounced at mRNA levels than at protein levels. This difference could be due to technical factors, such as the methods used to detect mRNA and proteins, to experimental errors, or to biological factors, such as RNA secondary structure, ribosome occupancy, and RNA and protein stability.

We analyzed BUB3 expression by using published databases from the publicly available UALCAN data portal (<http://ualcan.path.uab.edu/index.html>) [16]. The results indicated an increase in BUB3 expression at transcription levels in GBM *versus* normal tissues, which, however, was not sufficient to reach statistical significance ( $p$  < 0.27) (Fig. 1C). Notably, BUB3 protein levels were increased in GBM tissues, with high statistical significance ( $p$  <  $6.32E-21$ ) (Fig. 1D). These results suggest that BUB3 overexpression is a common feature in GBM, which could impact the SAC activity and, consequently, aneuploidy rate and tumor progression and aggressiveness.

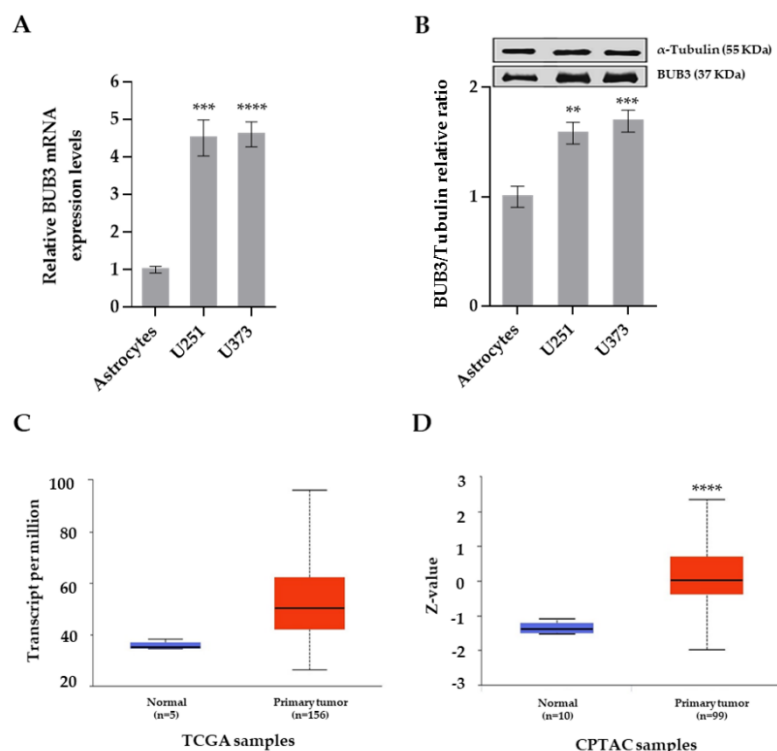


**Figure 1. BUB3 is upregulated in glioblastoma multiforme.** (A) Relative expression of BUB3 mRNA, as determined by qRT-PCR in U251 and U373 glioblastoma cell lines, comparatively to non-tumor astrocytes. (B) Representative immunoblots showing an increase of BUB3 protein levels in glioblastoma cell lines comparatively to astrocytes, and the respective quantification.  $\alpha$ -Tubulin was used as a loading control. (C-D) BUB3 expression at transcription (C) and protein (D) levels in glioblastoma *versus* normal tissues, retrieved from the UALCAN database. Statistical analysis was performed using Student t-test. \*\* $p < 0.01$ , \*\*\* $p < 0.001$  and \*\*\*\* $p < 0.0001$ . The error bars represent mean  $\pm$  SD. TCGA: The Cancer Genome Atlas, CPTAC: Clinical Proteomic Tumor Analysis Consortium.

### BUB3 knockdown interferes with proliferation of glioblastoma cells

To evaluate the effect of BUB3 inhibition, we first validated that RNAi-mediated knockdown of *BUB3* was effective in abolishing BUB3 protein production in the U251 and U373 glioblastoma cell lines. The immunofluorescent levels of BUB3 were diminished to undetectable levels ( $< 5\%$  of the levels of control siRNA-transfected cells), as judged by BUBR1 staining (due to the absence of anti-BUB3 antibodies that reproducibly label BUB3 at the kinetochores, we used an anti-BUBR1 antibody, as BUBR1 depends on BUB3 for kinetochore localization) (Fig. 2A). BUB3 protein levels were diminished to  $< 15\%$  of control siRNA-transfected cells (Fig. 2B). Also, BUB3-depleted cells exhibited incomplete metaphase plates, with persistent misaligned chromosomes, a phenotype reminiscent of the role known for BUB3 in kinetochore-to-microtubule attachments (Fig. 2A) [10,12]. Moreover, interphase nuclei of BUB3-depleted glioblastoma cells had irregular morphology, in contrast to the round-shaped nuclei of control siRNA-treated cells, indicative of aberrant chromosome segregation at anaphase (Fig. 2C).

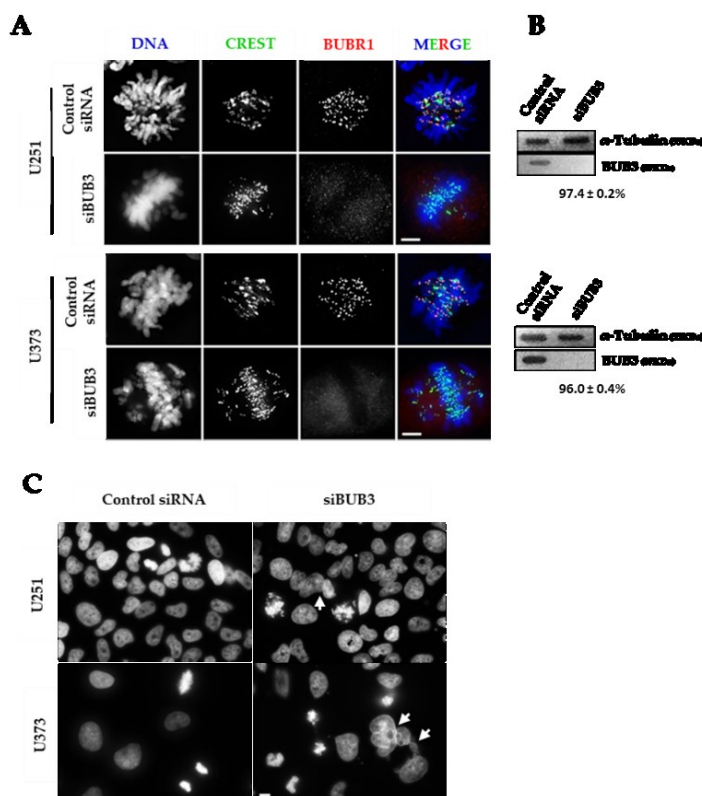


**Figure 2. RNAi-mediated BUB3 depletion is effective in U251 and U373 glioblastoma cell lines.** (A) Representative immunofluorescence images of U251 and U373 cells treated with control (control siRNA) and BUB3 (siBUB3) siRNAs for 72 hours and immunostained for CREST (green) and BUBR1 (red), showing BUBR1 absence from kinetochores in siBUB3-treated cells. DNA (blue) was stained with DAPI. Bar = 5  $\mu$ m. (B) Immunoblots from U251 and U373 cell lysates, showing effective repression of BUB3 (97.4 and 96.0%, respectively) after RNAi-mediated depletion.  $\alpha$ -Tubulin was used as a loading control. (C) U251 and U373 cells were stained for DNA with DAPI, showing irregular nuclei morphology (white arrows), after BUB3 depletion, resulting from premature exit from mitosis. Bar = 5  $\mu$ m.

Then, we analyzed the effect of BUB3 inhibition on cell growth of the two glioblastoma cell lines, either alone or in combination with paclitaxel. Paclitaxel was used at concentrations ranging from 1 to 10 nM. Paclitaxel concentrations < 100 nM in cell culture are considered as clinically relevant, corresponding to the intratumoral concentrations after treatment in the patients' tumor tissue [17,18]. Cells were exposed for 72 hours to 6.7 nM of siRNA against BUB3, or paclitaxel, or a combination of both; then, cell viability was determined by the MTT assay. We required a  $p$  value < 0.05 and a decrease in cell viability to less than 70% of the control levels. Knockdown of BUB3 decreased cell viability to less than 60% of control levels, in both glioblastoma cell lines (Fig. 3A and B). In contrast, there was little variation in cell viability after exposure to paclitaxel alone, at all concentrations tested, for the U373 cell line (Fig. 3B); for the U251 line, cell viability decreased to less than 70% at paclitaxel concentrations above 4 nM (Fig. 3A). The combination of BUB3 depletion with paclitaxel did not result in enhanced cytotoxicity, with the decrease in cell viability being close to that observed in cells treated with BUB3 siRNAs alone. BUB3 depletion and 10 nM paclitaxel individual exposures induced a slight increase in TUNEL-positive cells ( $1.2 \pm 0.3\%$  and  $1.6 \pm 0.5\%$ , respectively), compared to control cultures ( $0.5 \pm 0.1\%$ ) (Fig. 3C and D). The combination did not result in a consistent enhancement of TUNEL-positive cells. Thus, BUB3 depletion and/or paclitaxel induce slight levels of apoptosis which, *per se*, could not account for the decrease in cell growth observed through the MTT viability assay. We could not observe any difference in the levels of apoptosis between the different experiments after the measurement of caspase 3 activity, probably due to the low levels of apoptosis, which would be below the detection threshold of the test (Fig. 3E and F).

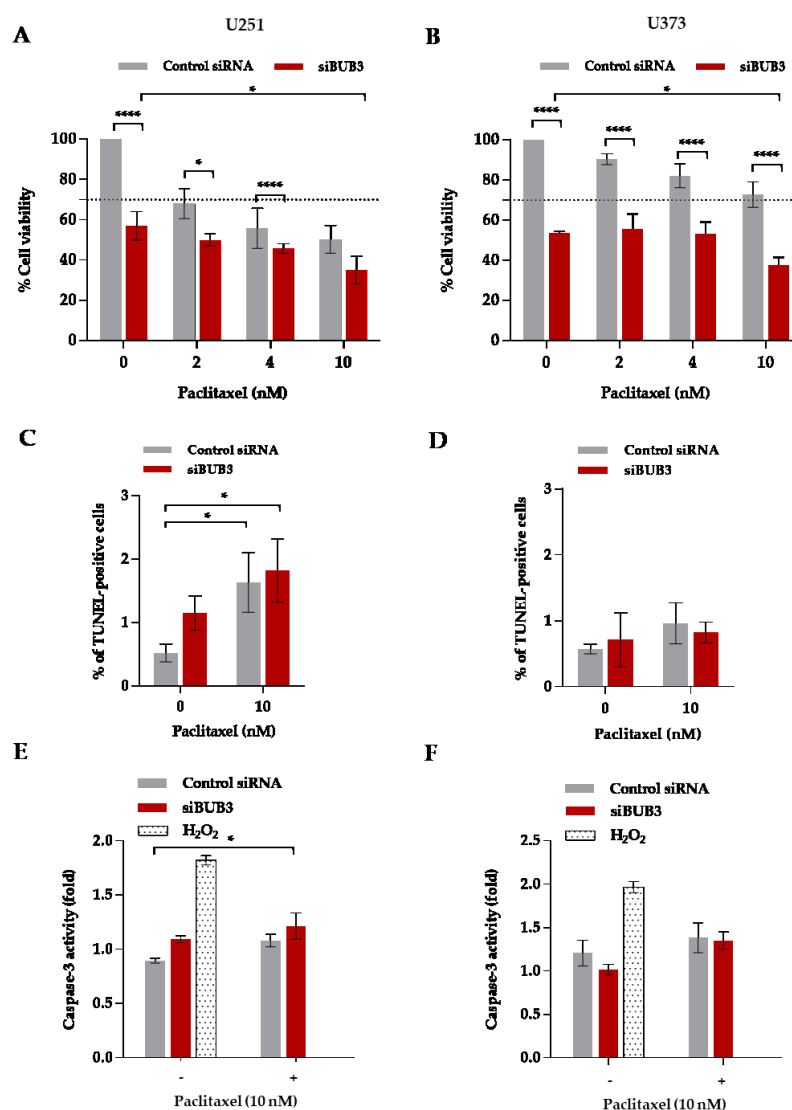


**Figure 3.** Effect of BUB3 knockdown and paclitaxel co-treatment on glioblastoma cell viability. U251 (A, C, E) and U373 (B, D, F) cells were transfected with control or BUB3 siRNAs for 24 hours. Then, paclitaxel was added at the indicated concentrations (0-10 nM). 48 hours later, we assessed cell viability (A-B), as determined by the MTT assay, the % of TUNEL-positive cells (C-D), and caspase 3 activity (E-F). \* $p < 0.05$ , \*\*\*\* $p < 0.0001$ , by two-way ANOVA with Tukey's multiple comparisons test. The error bars represent mean  $\pm$  SD.

Careful examination of cell morphology under fluorescence microscopy revealed accumulation of interphase nuclei with irregular shape and size, mainly multinucleated, in BUB3-RNAi and paclitaxel individually exposed cells, while regular round-shaped nuclei were observed in control cells (Fig. 4). BUB3-RNAi + paclitaxel combination exacerbated the accumulation of multinucleated cells in both cancer cell lines (Fig. 4). Cells with irregular nuclear shape and multinucleated cells may arise from aberrant cell division, which reflects loss and gain of chromosomes, producing aneuploid progeny. Nanomolar concentrations of paclitaxel were previously reported to induce multipolar spindles, which produce aneuploidy following aberrant cell division [17]. Such aneuploid cells exhibit a slow death kinetics, and the effect of paclitaxel is only apparent once a large proportion of the cell population has undergone aberrant, lethal mitoses, which may not occur during the first divisions [17]. Thus, it is possible that the time course of our experiments was not long enough to allow time for the BUB3-RNAi and/or paclitaxel treatments to exert their effect. Therefore, in the next section, we analyzed the effect of these treatments over a longer time course, of 10 days.

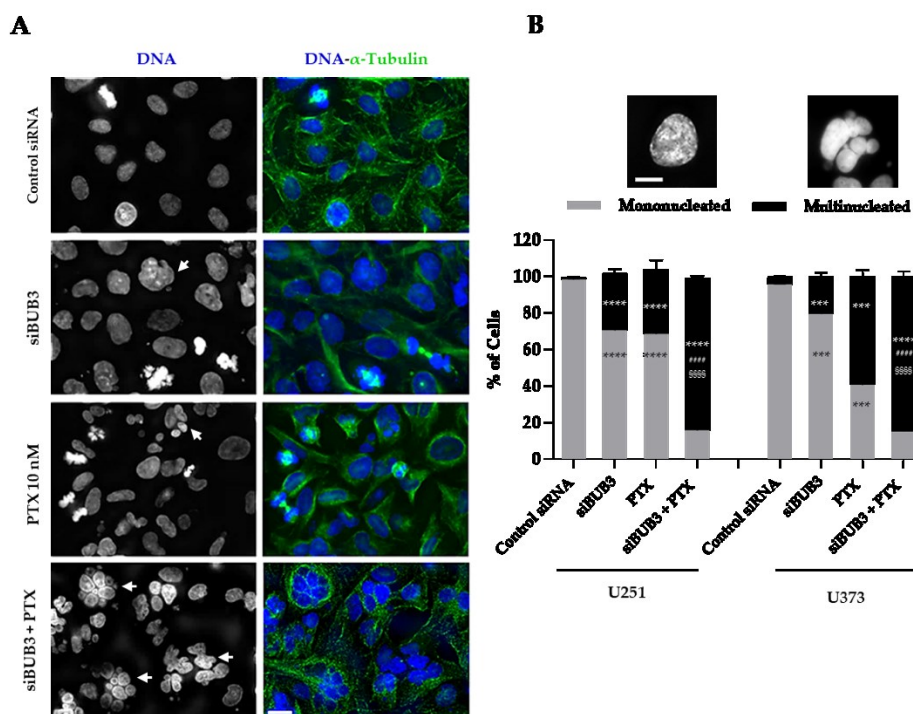


**Figure 4. Co-treatment with siRNA-BUB3 and paclitaxel induces accumulation of multinucleated cells in U251 and U373 glioblastoma cells.** (A) Representative immunofluorescence images of U251 cells exposed to control (Control siRNA) or BUB3 siRNAs (siBUB3) for 72 hours, either alone or in combination with 10 nM of paclitaxel (PTX). Cells were immunostained for  $\alpha$ -tubulin, to visualize microtubules (green), and the DNA (blue) was stained with DAPI, showing several multinucleated cells (white arrows) after the siBUB3 + PTX treatment, comparatively to Control siRNA-, siBUB3- or PTX-treated cells. Bar = 5  $\mu$ m. (B) Quantification (graph) of nuclear morphology (upper images, DAPI staining) in U251 and U373 cells treated as in (A). \*\*\*\* $p$  < 0.0001, siBUB3 + PTX or PTX or siBUB3 vs. Control siRNA; #### $p$  < 0.0001, siBUB3 + PTX vs. siBUB3; §§§§ $p$  < 0.0001 siBUB3 + PTX vs. PTX, by two-way ANOVA with Tukey's multiple comparisons test. The error bars represent mean  $\pm$  SD.

#### Inhibition of BUB3 impairs glioblastoma cell proliferation by exacerbating multipolar spindle phenotype induced by low doses of paclitaxel

To evaluate the effect of BUB3 inhibition, alone or in combination with paclitaxel, over a longer time course, we assessed the impact of the different treatments on the colony-forming ability of cells plated at low density and grown for 10 days. Colony formation was inhibited after BUB3 depletion or 4 nM paclitaxel single treatments, in both U251 and U373 cells (Fig. 5A and B). Further inhibition was achieved when combining BUB3 depletion with concentrations as low as 2 nM paclitaxel (Fig. 5A and B). Thus, combining BUB3 inhibition with clinically relevant concentrations of paclitaxel potentiates the antiproliferative activity on glioblastoma cells in a long-term run.

We sought to understand the mechanistic behind the antiproliferative activity of the combinatorial exposures. First, we analyzed the duration of the mitotic arrest in paclitaxel-treated cells, with and without BUB3 inhibition, by measuring the time from cell rounding to the flattening of the first daughter cell, as well as the cell fates of the treated cells, over 72 hours, by time-lapse microscopy. Previous studies reported that concentrations up to 10 nM paclitaxel induced a short mitotic delay (< 5 hours) in MDA-MB-231 and Cal51 breast cancer cells, while higher concentrations (up to 10  $\mu$ M) induced longer mitotic delay, up to 25 hours [17]. Our analysis showed that BUB3 depletion only did not affect mitotic duration, with siBUB3 siRNA-treated U251 cells behaving similarly to controls (Fig. 5C). Treatment with 10 nM paclitaxel resulted in a ~4 hour-mitotic delay, in accordance with previous studies [17]. Interestingly, this paclitaxel-induced delay was abolished in cells that were also depleted of BUB3, as a result of SAC deficiency, rendering the cells unable to sustain the mitotic delay [19,20]. As to cell fates, we found that apart from few abnormal cell divisions (10.4%) and apoptosis (8.3%), most BUB3-inhibited cells (81.3%) proceeded to apparently normal cell division, similarly to control cells (100%) (Fig. 5D). Most of paclitaxel-treated cells (78.3%) underwent aberrant cell division, with cell death occurring only marginally (13.0%). BUB3-RNAi + paclitaxel combination resulted in a slight but not significant increase in cell death (32.5%), at the expense of a diminution of abnormal cell division (52.5%), comparatively to paclitaxel alone (78.3%) (Fig. 5D). Overall, although cell division is affected by the individual and combined treatments, in terms of SAC activity, duration, and aberrant divisions, the effect of these defects on cell viability could not be apparent in a short-term run.

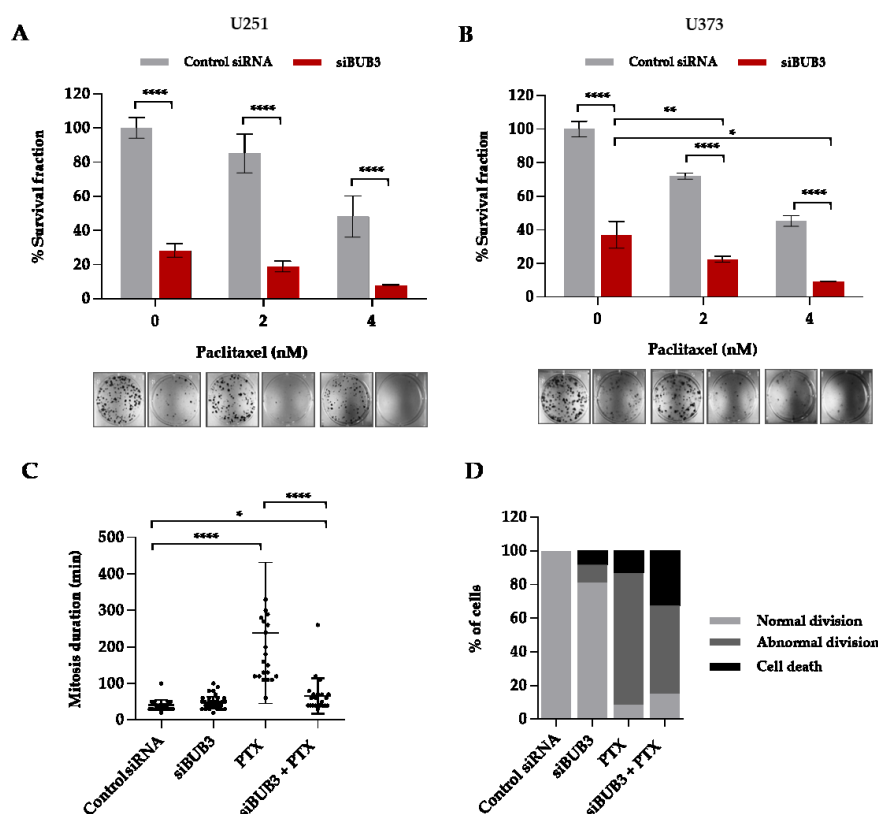


**Figure 5. Co-treatment with BUB3 siRNAs and paclitaxel impairs glioblastoma cell proliferation, in a long-term assay.** U251 (A) and U373 (B) cells were treated with control (Control siRNA) or BUB3 (siBUB3) siRNAs for 72 hours, either alone or in combination with paclitaxel (PTX, 2 and 4 nM), washed and allowed to grow for 10 days for colony formation assay. Results are expressed as % of survival fraction. Representative images of surviving colonies (bottom) are shown for each condition. (C) Quantification of mitosis duration, after time-lapse imaging for 72 hours, of U251 cells treated with control (Control siRNA) or BUB3 (siBUB3) siRNAs, alone or in combination with paclitaxel (PTX, 10 nM). Each spot represents one cell. Statistical analysis was performed by Kruskal–Wallis with Dunn’s multiple correction test. The error bars represent mean  $\pm$  SD. Control siRNA ( $n = 31$ ), siBUB3 ( $n = 48$ ), PTX ( $n = 22$ ), siBUB3 + PTX ( $n = 23$ ). (D) Graphic representation of cell fate represented in (A).

Cancer cells treated with low nanomolar doses of paclitaxel were previously reported to develop multipolar spindles, responsible for abnormal mitosis [17,21]. Such alteration in spindle morphology is due to diminished microtubule dynamics, because paclitaxel low doses ( $\leq 100$  nM) potently and selectively suppress the rate and extent of shortening at plus ends [22]. We thus performed immunofluorescence staining with anti-tubulin antibodies to visualize the mitotic spindle in treated cells. As expected, most of mitotic spindles ( $53.6 \pm 4.0\%$  and  $84.8 \pm 5.8\%$  in U251 and U373, respectively) in paclitaxel-treated cells were multipolar, while spindles had bipolar appearance in controls ( $96.1 \pm 1.0\%$  and  $96.6 \pm 0.8\%$  in U251 and U373, respectively) and BUB3-depleted U251 ( $95.8 \pm 2.0\%$ ) and U373 ( $94.2 \pm 0.1\%$ ) cells (Fig. 6). Multipolar spindles were further increased after treatment with the BUB3-RNAi + paclitaxel combination, in both U251 ( $62.2 \pm 2.0\%$ ) and U373 ( $98.2 \pm 1.1\%$ ) cells (Fig. 6). Depletion of BUB3 in paclitaxel-treated cells may have two consequences: i) depletion of BUB3 generates instable kinetochore-microtubule attachments, which contribute to the multipolar spindle phenotype, as stable bipolar attachments are required to form a stable bipolar spindle; and ii) depletion of BUB3 delays chromosome alignment at the metaphase plate, which would increase the rate of loss and gain of chromosomes. Both multipolar spindles and delayed chromosome alignment at the spindle equator increase the rate of chromosome missegregation and aneuploidy [21,23]. On the other hand, increased aneuploidy over successive divisions is lethal to cancer cells, as enhanced chromosome missegregation limits survival of aneuploid cancer cells [24–27].

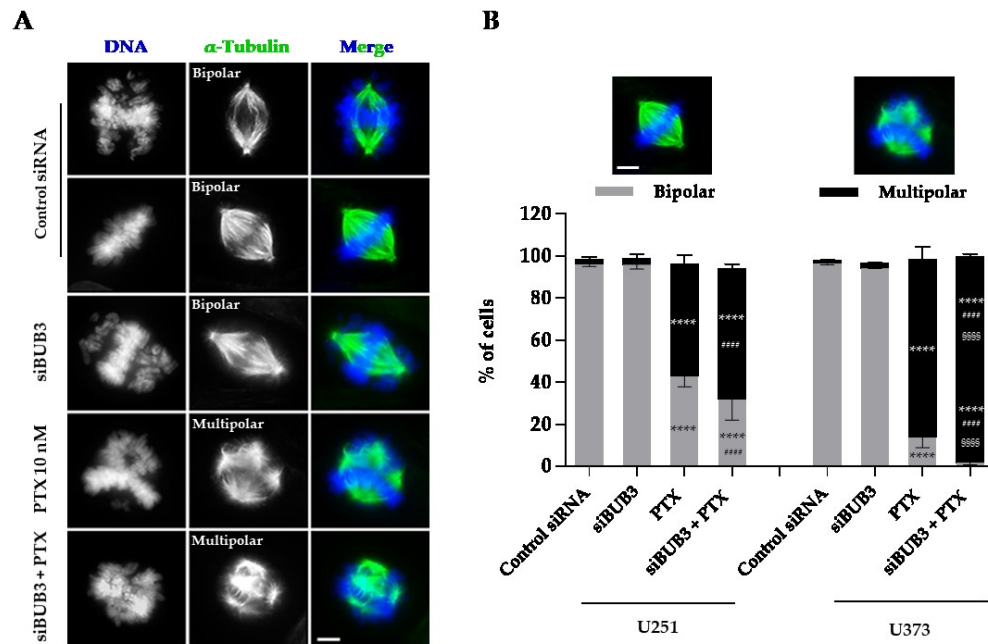


**Figure 6. BUB3 knockdown potentiates the multipolar spindle phenotype induced by paclitaxel treatment in U251 and U373 glioblastoma cells.** (A) Representative immunofluorescence images of U251 cells treated with control (Control siRNA) or BUB3 siRNAs (siBUB3) for 72 hours, either alone or in combination with 10 nM of paclitaxel (PTX). Cells were immunostained for  $\alpha$ -tubulin, to visualize microtubules (green), and the DNA (blue) was stained with DAPI. Bar = 5  $\mu$ m. (B) Quantification (graph) of spindle morphology (upper images, DNA - blue, and mitotic spindle - green) in U251 and U373 cells treated as in (A). \*\*\*\* $p$  < 0.0001, siBUB3 + PTX or siBUB3 vs. Control siRNA; ##### $p$  < 0.0001, siBUB3 + PTX vs. siBUB3; §§§§ $p$  < 0.0001, siBUB3 + PTX vs. PTX, by two-way ANOVA with Tukey's multiple comparisons test. The error bars represent mean  $\pm$  SD.

### BUB3 downregulation induces cellular senescence in glioblastoma cells, which is exacerbated by co-treatment with paclitaxel

We were intrigued by the low levels of apoptosis observed after BUB3-depletion and/or paclitaxel treatments. BUB3 was previously involved in premature aging, and shares extensive sequence homology with each of the four WD repeat motifs and over the entire length of the ribonucleic acid export 1 (RAE1) protein, also involved in premature aging [28,29]. We thus suspected cellular senescence as a possible alternative process to explain the results obtained in the colony-forming assay (CFA). Cellular senescence is considered an alternative tumor suppressor mechanism [30,31]. Senescent cells develop morphological and structural changes, including an enlarged, flattened, multinucleated morphology with altered composition of the plasma membrane and a remarkable nuclear enlargement [32]. A characteristic feature of senescent cells is increased lysosomal SA- $\beta$ -gal activity [33].

Observation of the crystal violet-stained CFA plates, under phase contrast microscopy, revealed the existence of cells with enlarged and flattened morphology and increased cytoplasmic granularity, reminiscent of senescent cells, after BUB3-depletion and 4 nM paclitaxel individual treatments (Fig. 7A). This senescence phenotype was more pronounced in CFA plates from BUB3-depletion and 4 nM paclitaxel combination treatment (Fig. 7A). The result was confirmed by the *in situ* SA- $\beta$ -gal assay, in both U251 and U373 cells (Fig. 7B and C). The results of this study suggest that BUB3 downregulation induces premature cellular senescence and, concomitantly with SAC weakening, increases the levels of a senescent phenotype involved in the paclitaxel response in glioblastoma cells.

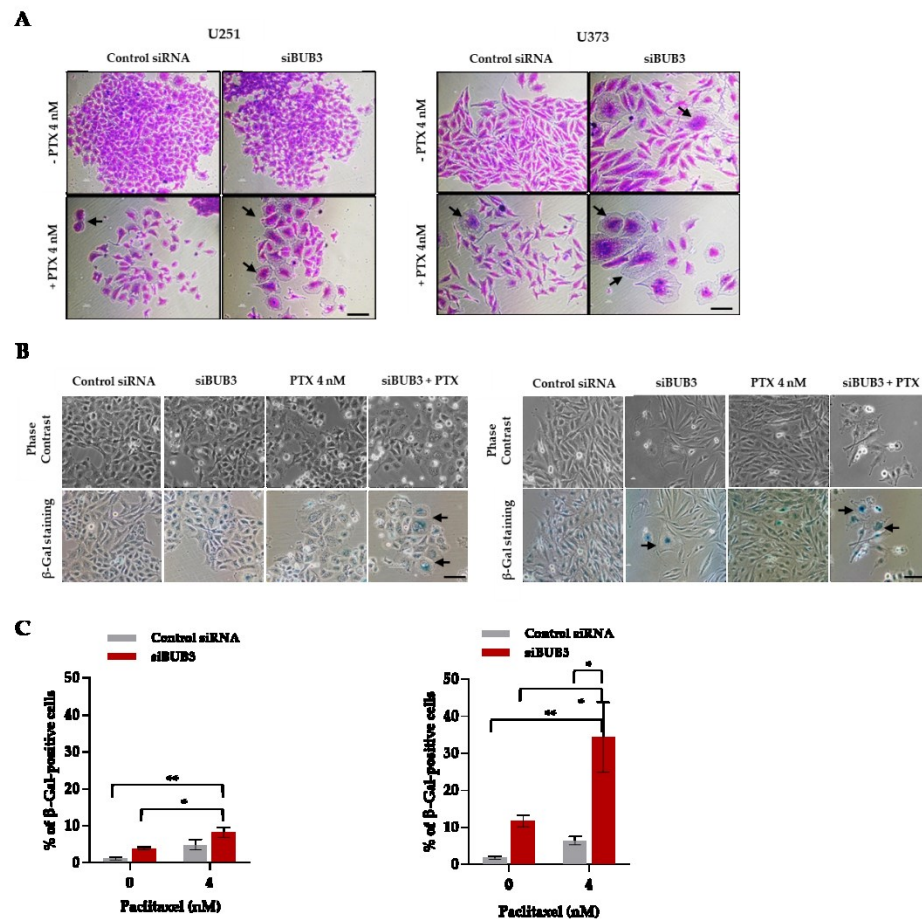


**Figure 7. Co-treatment with BUB3-siRNAs and paclitaxel induces cellular senescence in U251 and U373 glioblastoma cells.** (A) Representative phase contrast microscopy images of crystal violet-stained colonies (see Materials and Methods for details), showing the presence of enlarged and flattened U251 and U373 cells (black arrows), pronounced after siBUB3 + paclitaxel (PTX) co-treatment. Bar = 20  $\mu$ m. (B) U251 (left) and U373 (right) cells were treated with control (Control siRNA) or BUB3 (siBUB3) siRNAs for 72 hours, either alone or in combination with 10 nM PTX and stained for SA- $\beta$ -gal, showing a presence of blue senescent cells (black arrows). (C) Quantification of the data presented in (B). \* $p < 0.05$ , \*\* $p < 0.01$ , by two-way ANOVA with Tukey's multiple comparisons test. The error bars represent mean  $\pm$  SD.

## Discussion

In the present study, we showed that the SAC gene *BUB3* is overexpressed in the glioblastoma cell lines studied, in agreement with the public database UALCAN (<http://ualcan.path.uab.edu/index.html>). We have characterized the effects of BUB3 downregulation and found it to inhibit the proliferation of glioblastoma cells. The antiproliferative effect was further enhanced when BUB3-depleted cells were also challenged with clinically relevant doses of paclitaxel. Apoptosis had only a slight contribution to this antiproliferative effect. We also found that single treatment with BUB3 depletion or paclitaxel induced cellular senescence of glioblastoma cells. Remarkably, synergistic senescence was achieved when glioblastoma cells were treated with the combination of BUB3 depletion and paclitaxel, making senescence the major mechanism of the antiproliferative effect of the combination (Fig. 8).

To the best of our knowledge, this is the first report of the induction of cellular senescence by BUB3 downregulation in human cancer cells. This is not surprising, as BUB3 shares extensive sequence homology with the RAE1 protein, which was involved in senescence induction [28,29]. Interestingly, mice harboring combined *Bub3* and *Rae1* haploinsufficiency exhibited reduced lifespan, associated with premature senescence [34–36]. Because senescent cells are cell cycle arrested, cellular senescence has been emerging as a desirable outcome during cancer treatment [37]. Therefore, targeting BUB3 could be a valuable strategy to induce cancer cell senescence. Nevertheless, one should be aware of the possible detrimental effects of senescent cells, including tumor promoting properties [37].

Paclitaxel also induces senescence in cancer cells [38]. Our study showed that BUB3 knockdown enhanced the cytotoxic effect of paclitaxel on glioblastoma cells, probably because of enhanced senescence. Failed mitosis was reported to induce multinucleated senescent cells [39]. In this sense, both BUB3 depletion and paclitaxel may induce failed mitosis and, consequently, promote senescence. Paclitaxel induces multipolar spindles, which may result in chromosome missegregation. BUB3 depletion enhances

the multipolar spindle phenotype of paclitaxel treatment, probably through SAC weakening, misaligned chromosomes, and premature exit from mitosis, thereby enhancing mitotic failure and aneuploidy [21,23]. This would create conditions that are favorable to both cell death and cellular senescence. Indeed, besides senescence, apoptosis was also induced by the BUB3 depletion plus paclitaxel combination, albeit to a lesser extent.

It is noteworthy that one could not expect that non-tumor cells will behave differently from glioblastoma cells in response to BUB3 depletion plus paclitaxel, as both microtubules (affected by paclitaxel) and BUB3 are required for proper cell division both in cancer and in non-cancer cells. Although it is also toxic to normal dividing cells, paclitaxel is one of the most widely used anticancer agents. Nowadays, the great challenge is to target paclitaxel (or other anticancer drugs) specifically to cancer cells (and not to normal cells) to minimize undesired toxicity. A valuable approach is to use functionalized nanoparticles to target cancer cells without disturbing normal cells [40,41].

In conclusion, we showed that *BUB3* is upregulated in GBM and glioblastoma cell lines, and that its downregulation induces a senescence-like phenotype accompanied by cell enlargement and increased SA- $\beta$ -gal activity. The senescent phenotype is enhanced after treatment with paclitaxel, indicating that senescence could be of great significance in inhibiting GBM development. We suggest that BUB3 could be used as a biomarker and new pharmacological target in the treatment for GBM.

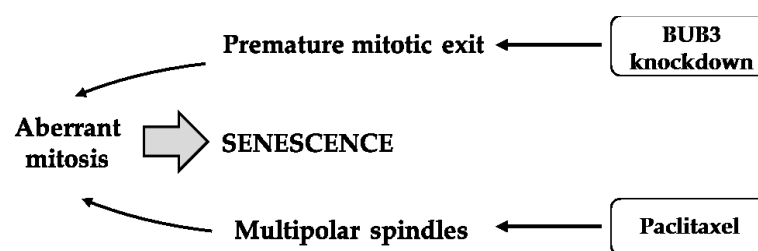


**Figure 8.** Combination of BUB3 depletion and paclitaxel to enhance senescence. Senescence can arise from aberrant mitosis. Aberrant mitosis can arise from premature mitotic exit after BUB3 knockdown, or from mitotic exit in the presence of multipolar spindles of cells exposed to nanomolar doses of paclitaxel. When the two treatments are combined, senescence is enhanced to a greater extent than with each treatment alone. As a result, the cells undergo sustained senescence.

### Acknowledgments

The authors acknowledge CESPU – Cooperativa de Ensino Superior Politécnico e Universitário for financial and technical support (projects AntiMitoSphere\_APSFCT\_IINFACTS\_2021). This work was partially supported by FCT- Fundação para a Ciência e a Tecnologia (grant PTDC/BIA-CEL/30014/2017; POCI-01-0145-FEDER-030014). We are grateful to all members of Hassan Bousbaa’s lab for their critical discussion of the present work.

### Author Contributions

HB and RMR conceived and designed the study. PMAS and AVN conducted the experiments. PMAS, AVN, OM, RMR and HB collected and analyzed experimental data. PMAS and HB drafted the manuscript. All authors revised the manuscript. HB and RMR supervised the work. HB acquired and managed the funding. All authors read and approved the final manuscript.

### Conflicts of interest

The authors declare no competing interests.

### References

1. Gritsch, S.; Batchelor, T.T.; Gonzalez Castro, L.N. Diagnostic, Therapeutic, and Prognostic Implications of the 2021 World Health Organization Classification of Tumors of the Central Nervous System. *Cancer* **2022**, *128*, 47–58, doi:10.1002/cncr.33918.
2. Lim, S.K.; Llaguno, S.R.A.; McKay, R.M.; Parada, L.F. Glioblastoma Multiforme: A Perspective on Recent Findings in Human Cancer and Mouse Models. *BMB Rep.* **2011**, *44*, 158–164, doi:10.5483/BMBRep.2011.44.3.158.
3. Stupp, R.; Mason, W.P.; van den Bent, M.J.; Weller, M.; Fisher, B.; Taphoorn, M.J.B.; Belanger, K.; Brandes, A.A.; Marosi, C.; Bogdahn, U.; et al. Radiotherapy plus Concomitant and Adjuvant Temozolomide for Glioblastoma. *N. Engl. J. Med.* **2005**, *352*, 987–996, doi:10.1056/NEJMoa043330.
4. Le Rhun, E.; Preusser, M.; Roth, P.; Reardon, D.A.; van den Bent, M.; Wen, P.; Reifenberger, G.; Weller, M. Molecular Targeted Therapy of Glioblastoma. *Cancer Treat. Rev.* **2019**, *80*, 101896, doi:10.1016/j.ctrv.2019.101896.

5. Raysi Dehcordi, S.; De Paulis, D.; Marzi, S.; Ricci, A.; Cimini, A.; Cifone, M.G.; Galzio, R.J. Survival Prognostic Factors in Patients with Glioblastoma: Our Experience. *J. Neurosurg. Sci.* **2012**, *56*, 239–245.
6. Kops, G.J.P.L.; Weaver, B.A.A.; Cleveland, D.W. On the Road to Cancer: Aneuploidy and the Mitotic Checkpoint. *Nat. Rev. Cancer* **2005**, *5*, 773–785, doi:10.1038/nrc1714.
7. Silva, P.; Barbosa, J.; Nascimento, A.V.; Faria, J.; Reis, R.; Bousbaa, H. Monitoring the Fidelity of Mitotic Chromosome Segregation by the Spindle Assembly Checkpoint. *Cell Prolif.* **2011**, *44*, doi:10.1111/j.1365-2184.2011.00767.x.
8. Hoyt, M.A.; Totis, L.; Roberts, B.T. S. *Cerevisiae* Genes Required for Cell Cycle Arrest in Response to Loss of Microtubule Function. *Cell* **1991**, *66*, 507–517, doi:10.1016/0092-8674(81)90014-3.
9. Wang, Y.; Burke, D.J. Checkpoint Genes Required to Delay Cell Division in Response to Nocodazole Respond to Impaired Kinetochores Function in the Yeast *Saccharomyces Cerevisiae*. *Mol. Cell. Biol.* **1995**, *15*, 6838–6844, doi:10.1128/MCB.15.12.6838.
10. Logarinho, E.; Resende, T.; Torres, C.; Bousbaa, H. The Human Spindle Assembly Checkpoint Protein Bub3 Is Required for the Establishment of Efficient Kinetochores-Microtubule Attachments. *Mol. Biol. Cell* **2008**, *19*, 1798–1813, doi:10.1091/mbc.e07-07-0633.
11. Reis, R.M.; Nakamura, M.; Masuoka, J.; Watanabe, T.; Colella, S.; Yonekawa, Y.; Kleihues, P.; Ohgaki, H. Mutation Analysis of HBUB1, HBUBR1 and HBUB3 Genes in Glioblastomas. *Acta Neuropathol.* **2001**, *101*, 297–304, doi:10.1007/s004010100366.
12. Logarinho, E.; Bousbaa, H. Kinetochores-Microtubule Interactions “in Check” by Bub1, Bub3 and BubR1: The Dual Task of Attaching and Signalling. *Cell Cycle* **2008**, *7*.
13. Silva, P.M.A.; Delgado, M.L.; Ribeiro, N.; Florindo, C.; Tavares, Á.A.; Ribeiro, D.; Lopes, C.; do Amaral, B.; Bousbaa, H.; Monteiro, L.S. Spindly and Bub3 Expression in Oral Cancer: Prognostic and Therapeutic Implications. *Oral Dis.* **2019**, *25*, 1291–1301, doi:10.1111/odi.13089.
14. Maia, A.R.R.; Linder, S.; Song, J.-Y.; Vaarting, C.; Boon, U.; Pritchard, C.E.J.; Velds, A.; Huijbers, I.J.; van Tellingen, O.; Jonkers, J.; et al. Mps1 Inhibitors Synergise with Low Doses of Taxanes in Promoting Tumour Cell Death by Enhancement of Errors in Cell Division. *Br. J. Cancer* **2018**, *118*, 1586–1595, doi:10.1038/s41416-018-0081-2.
15. Wengner, A.M.; Siemeister, G.; Koppitz, M.; Schulze, V.; Kosemund, D.; Klar, U.; Stoeckigt, D.; Neuhaus, R.; Lienau, P.; Bader, B.; et al. Novel Mps1 Kinase Inhibitors with Potent Antitumor Activity. *Mol. Cancer Ther.* **2016**, *15*, 583–592, doi:10.1158/1535-7163.MCT-15-0500.
16. Chandrashekar, D.S.; Bashel, B.; Balasubramanya, S.A.H.; Creighton, C.J.; Ponce-Rodriguez, I.; Chakravarthi, B.V.S.K.; Varambally, S. UALCAN: A Portal for Facilitating Tumor Subgroup Gene Expression and Survival Analyses. *Neoplasia* **2017**, *19*, 649–658, doi:10.1016/j.neo.2017.05.002.
17. Zasadil, L.M.; Andersen, K.A.; Yeum, D.; Rocque, G.B.; Wilke, L.G.; Tevaarwerk, A.J.; Raines, R.T.; Burkard, M.E.; Weaver, B.A. Cytotoxicity of Paclitaxel in Breast Cancer Is Due to Chromosome Missegregation on Multipolar Spindles. *Sci. Transl. Med.* **2014**, *6*, 229ra43, doi:10.1126/scitranslmed.3007965.
18. Weaver, B.A. How Taxol/Paclitaxel Kills Cancer Cells. *Mol. Biol. Cell* **2014**, *25*, 2677–2681, doi:10.1091/mbc.E14-04-0916.
19. Yang, Z.; Kenny, A.E.; Brito, D.A.; Rieder, C.L. Cells Satisfy the Mitotic Checkpoint in Taxol, and Do so Faster in Concentrations That Stabilize Syntelic Attachments. *J. Cell Biol.* **2009**, *186*, 675–684, doi:10.1083/jcb.200906150.
20. Brito, D.A.; Yang, Z.; Rieder, C.L. Microtubules Do Not Promote Mitotic Slippage When the Spindle Assembly Checkpoint Cannot Be Satisfied. *J. Cell Biol.* **2008**, *182*, 623–629, doi:10.1083/jcb.200805072.
21. Silkworth, W.T.; Nardi, I.K.; Scholl, L.M.; Cimini, D. Multipolar Spindle Pole Coalescence Is a Major Source of Kinetochores Mis-Attachment and Chromosome Mis-Segregation in Cancer Cells. *PLoS One* **2009**, *4*, e6564, doi:10.1371/journal.pone.0006564.
22. Derry, W.B.; Wilson, L.; Jordan, M.A. Substoichiometric Binding of Taxol Suppresses Microtubule Dynamics. *Biochemistry* **1995**, *34*, 2203–2211, doi:10.1021/bi00007a014.
23. Kuniyasu, K.; Iemura, K.; Tanaka, K. Delayed Chromosome Alignment to the Spindle Equator Increases the Rate of Chromosome Missegregation in Cancer Cell Lines. *Biomolecules* **2018**, *9*, doi:10.3390/biom9010010.
24. Kawakami, M.; Liu, X.; Dmitrovsky, E. New Cell Cycle Inhibitors Target Aneuploidy in Cancer Therapy. *Annu. Rev. Pharmacol. Toxicol.* **2019**, *59*, 361–377, doi:10.1146/annurev-pharmtox-010818-021649.

25. Birkbak, N.J.; Eklund, A.C.; Li, Q.; McClelland, S.E.; Endesfelder, D.; Tan, P.; Tan, I.B.; Richardson, A.L.; Szallasi, Z.; Swanton, C. Paradoxical Relationship between Chromosomal Instability and Survival Outcome in Cancer. *Cancer Res.* **2011**, *71*, 3447–3452, doi:10.1158/0008-5472.CAN-10-3667.
26. Komarova, N.L.; Wodarz, D. The Optimal Rate of Chromosome Loss for the Inactivation of Tumor Suppressor Genes in Cancer. *Proc. Natl. Acad. Sci. U. S. A.* **2004**, *101*, 7017–7021, doi:10.1073/pnas.0401943101.
27. Giam, M.; Rancati, G. Aneuploidy and Chromosomal Instability in Cancer: A Jackpot to Chaos. *Cell Div.* **2015**, *10*, 3, doi:10.1186/s13008-015-0009-7.
28. Taylor, S.S.; Ha, E.; McKeon, F. The Human Homologue of Bub3 Is Required for Kinetochore Localization of Bub1 and a Mad3/Bub1-Related Protein Kinase. *J. Cell Biol.* **1998**, *142*, 1–11, doi:10.1083/jcb.142.1.1.
29. Martinez-Exposito, M.J.; Kaplan, K.B.; Copeland, J.; Sorger, P.K. Retention of the BUB3 Checkpoint Protein on Lagging Chromosomes. *Proc. Natl. Acad. Sci. U. S. A.* **1999**, *96*, 8493–8498, doi:10.1073/pnas.96.15.8493.
30. Collado, M.; Serrano, M. The Senescent Side of Tumor Suppression. *Cell Cycle* **2005**, *4*, 1722–1724, doi:10.4161/cc.4.12.2260.
31. Courtois-Cox, S.; Jones, S.L.; Cichowski, K. Many Roads Lead to Oncogene-Induced Senescence. *Oncogene* **2008**, *27*, 2801–2809, doi:10.1038/sj.onc.1210950.
32. Kumari, R.; Jat, P. Mechanisms of Cellular Senescence: Cell Cycle Arrest and Senescence Associated Secretory Phenotype. *Front. cell Dev. Biol.* **2021**, *9*, 645593, doi:10.3389/fcell.2021.645593.
33. Kurz, D.J.; Decary, S.; Hong, Y.; Erusalimsky, J.D. Senescence-Associated (Beta)-Galactosidase Reflects an Increase in Lysosomal Mass during Replicative Ageing of Human Endothelial Cells. *J. Cell Sci.* **2000**, *113* (Pt 2), 3613–3622.
34. Babu, J.R.; Jeganathan, K.B.; Baker, D.J.; Wu, X.; Kang-Decker, N.; van Deursen, J.M. Rael Is an Essential Mitotic Checkpoint Regulator That Cooperates with Bub3 to Prevent Chromosome Missegregation. *J. Cell Biol.* **2003**, *160*, 341–353, doi:10.1083/jcb.200211048.
35. Dai, W.; Wang, X. Aging in Check. *Sci. Aging Knowledge Environ.* **2006**, *2006*, pe9, doi:10.1126/sageke.2006.7.pe9.
36. Baker, D.J.; Jeganathan, K.B.; Malureanu, L.; Perez-Terzic, C.; Terzic, A.; van Deursen, J.M.A. Early Aging-Associated Phenotypes in Bub3/Rael Haploinsufficient Mice. *J. Cell Biol.* **2006**, *172*, 529–540, doi:10.1083/jcb.200507081.
37. Sieben, C.J.; Sturmlechner, I.; van de Sluis, B.; van Deursen, J.M. Two-Step Senescence-Focused Cancer Therapies. *Trends Cell Biol.* **2018**, *28*, 723–737, doi:10.1016/j.tcb.2018.04.006.
38. Bargiela-Iparraguirre, J.; Prado-Marchal, L.; Pajuelo-Lozano, N.; Jiménez, B.; Perona, R.; Sánchez-Pérez, I. Mad2 and BubR1 Modulates Tumorigenesis and Paclitaxel Response in MKN45 Gastric Cancer Cells. *Cell Cycle* **2014**, *13*, 3590–3601, doi:10.4161/15384101.2014.962952.
39. Dikovskaya, D.; Cole, J.J.; Mason, S.M.; Nixon, C.; Karim, S.A.; McGarry, L.; Clark, W.; Hewitt, R.N.; Sammons, M.A.; Zhu, J.; et al. Mitotic Stress Is an Integral Part of the Oncogene-Induced Senescence Program That Promotes Multinucleation and Cell Cycle Arrest. *Cell Rep.* **2015**, *12*, 1483–1496, doi:10.1016/j.celrep.2015.07.055.
40. Nascimento, A.V.; Singh, A.; Bousbaa, H.; Ferreira, D.; Sarmiento, B.; Amiji, M.M. Mad2 Checkpoint Gene Silencing Using Epidermal Growth Factor Receptor-Targeted Chitosan Nanoparticles in Non-Small Cell Lung Cancer Model. *Mol. Pharm.* **2014**, *11*, 3515–3527, doi:10.1021/mp5002894.
41. Nascimento, A.V.; Singh, A.; Bousbaa, H.; Ferreira, D.; Sarmiento, B.; Amiji, M.M. Overcoming Cisplatin Resistance in Non-Small Cell Lung Cancer with Mad2 Silencing siRNA Delivered Systemically Using EGFR-Targeted Chitosan Nanoparticles. *Acta Biomater.* **2017**, *47*, 71–80, doi:10.1016/j.actbio.2016.09.045.



In *Scientific Letters*, articles are published under a CC-BY license (Creative Commons Attribution 4.0 International License at <https://creativecommons.org/licenses/by/4.0/>), the most open license available. The users can share (copy and redis-

tribute the material in any medium or format) and adapt (remix, transform, and build upon the material for any purpose, even commercially), as long as they give appropriate credit, provide a link to the license, and indicate if changes were made (read the full text of the license terms and conditions of use at <https://creativecommons.org/licenses/by/4.0/legalcode>).